Charging Current in Long Lines and High-Voltage Cables – Protection Application Considerations

Yiyan Xue
American Electric Power

Dale Finney and Bin Le
Schweitzer Engineering Laboratories, Inc.

Presented at the
67th Annual Georgia Tech Protective Relaying Conference
Atlanta, Georgia
May 8–10, 2013

Originally presented at the
39th Annual Western Protective Relay Conference, October 2012

Charging Current in Long Lines and High-Voltage Cables – Protection Application Considerations

Yiyan Xue, *American Electric Power*
Dale Finney and Bin Le, *Schweitzer Engineering Laboratories, Inc.*

***Abstract*—In the analysis of power line protection behavior, the series impedance of the lumped parameter line model is often sufficient because the impact of the shunt capacitance is not significant. However, when long transmission overhead lines or underground cables are present in the system, the effects of the charging current caused by the shunt capacitance need to be considered. This current flows onto the protected line or cable from all terminals. Its impacts are present during normal operation and during system transients. Due to the symmetry of the line impedances, the charging currents can be relatively equal in each phase in the steady state. Thus the negative- and zero-sequence components will be small—an advantage when applying relays that operate for sequence components. However, the charging current during line energization, internal faults, and external faults will differ from steady-state values. This paper explores the impact of charging current on the various types of protection elements employed to protect line and cable circuits. It reviews methods used to mitigate the effects of charging current and provides general guidance on settings.**

I. Principles of High-Voltage Line Protection

We begin this paper with a review of the basic operating principles of those relays typically applied for line or cable protection. Distance relays are widely used for line protection. In a mho-type distance element (see Fig. 1), the operating signal generally takes the form I • Z – V. It is inherently directional, owing to polarization by a voltage measurement. The underreaching distance element (Zone 1) is carefully designed to limit transient overreach. Consequently, it can be applied for instantaneous tripping without a communications channel. Practically, the Zone 1 distance reach (*m*) is typically set to 85 to 90 percent of the line to account for instrument transformer inaccuracy, relay manufacturing tolerances, and line impedance uncertainty. The element characteristic angle (eca) is set to match the line impedance angle.

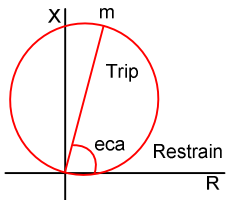

Fig. 1. Distance characteristic

Overreaching distance elements are also applied in conjunction with a communications channel. Transient overreach is inconsequential because relays at all terminals need to agree on the trip decision. However, the scheme is dependent on the availability of the channel.

The directional overcurrent relay is similar to the distance relay in that it makes a decision on fault direction through the measurement of local loop voltages and currents. The operating signal is the locally measured terminal current in the form of phase quantities or sequence components. Directionality is provided either by a polarizing current or voltage. The directional element characteristic is shown in Fig. 2. The element produces a positive indication of a fault; however, because it does not have a definite forward reach, it must be used in conjunction with a communications channel in order to provide selective protection.

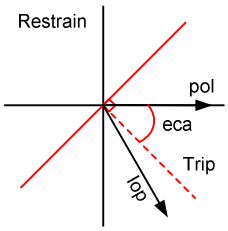

Fig. 2. Directional characteristic

Another category of line protection is the current-only scheme. This category includes phase comparison and current differential relays. In a phase comparison scheme, the operating signal is the local current. Polarities of the local and remote currents are exchanged and compared using a communications channel to determine if the fault is internal. Fig. 3 illustrates the phase comparison characteristic. Conceptually, the transmitted signal is a square wave with rising and falling edges that correspond with the positive and negative zero crossings of the local waveform. A timer accounts for phenomena that prevent a perfect coincidence of the local and remote currents [1]. This is presented as the blocking angle (ba) in Fig. 3.

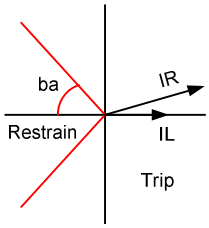

Fig. 3. Phase comparison characteristic

In a current differential scheme, the current magnitudes and angles are exchanged through the digital communications channel. The summation of local and remote current gives a positive identification of an internal fault. The scheme is more

sensitive than phase comparison. However, the security of the scheme can be negatively impacted by current transformer (CT) saturation. As a result, common implementations employ either a percentage differential or Alpha Plane characteristic.

A percentage differential element (see Fig. 4) operates when the differential signal exceeds the pickup threshold, which is biased by a percentage of the restraint signal—usually defined as the scalar sum of the currents flowing into the zone.

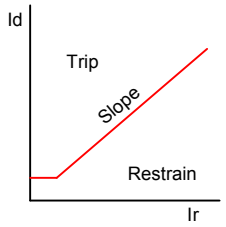

Fig. 4. Percentage differential characteristic

The Alpha Plane differential element responds to the absolute magnitude of the differential current for overcurrent supervision and to the complex ratio k = IL/IR for tripping or restraining. The latter measurement is applied to the characteristic shape shown in Fig. 5. This allows the magnitude and angle differences to be treated separately. The characteristic shape is set to provide security for channel synchronization errors and CT saturation.

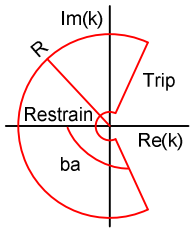

Fig. 5. Alpha Plane characteristic

Each of the principles described thus far can be implemented using the loop currents that flow during a fault. However, in general, these implementations can suffer a reduction in sensitivity for resistive faults under a load condition. As a result, variations of the directional, phase comparison, and differential elements are often implemented that respond to zero- and/or negative-sequence components. Zero-sequence elements operate for faults involving ground. Negative-sequence elements operate for all unbalanced faults. Because these elements do not see balanced loading, they offer much better sensitivity. As we will see, they are also impacted to a lesser degree by charging current.

II. Characterization of Charging Current

Next, we turn to the phenomenon of charging current to characterize it in terms of the magnitude of its phase and sequence components.

A. Calculation of Shunt Capacitance of a Line or Cable

In general, the two arbitrarily spaced conductors shown in Fig. 6 exhibit capacitance with each other due to the potential difference between them.

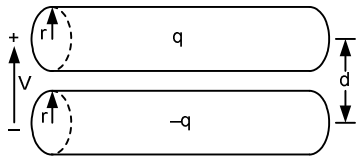

Fig. 6. Potential and charges of two conductors

Assuming two parallel conductors with a distance d and each with a radius r are energized by a voltage source, both will carry charges of q coulombs. Derived from Gauss's law on the relationship between electric charges and electric fields [2], the potential difference between the two conductors is calculated by the following:

$$V = \frac{q}{\pi\varepsilon}\ln\frac{d}{r} \tag{1}$$

where:

ε = the permittivity of dielectric between the conductors.

For overhead transmission lines, the permittivity of air is approximately equal to the dielectric constant of a vacuum, $\varepsilon = \varepsilon_0 = 8.854 \bullet 10^{-12}$ F per meter. From (1) and by definition, the capacitance between two conductors in unit length is:

$$C = \frac{q}{V} = \frac{\pi\varepsilon}{\ln\frac{d}{r}} \tag{2}$$

Equation (2) is the general formula to calculate capacitance. Depending on the structures and geometry of the line or cable, the parameters d and r in (2) will be defined differently. But this general formula tells us that the capacitance of an overhead line is determined by the conductor size, the spacing (between conductors and between a conductor and ground), and the total length of the line. For a cable, the permittivity ε of the dielectric around the conductors is generally two to four times the dielectric constant ε_0. In addition, the spacing between each cable conductor and ground is usually much smaller than that of an overhead line, so the cable will exhibit much higher capacitance than an overhead line with the same length.

In a typical three-phase power system, because there are potential differences between the phase conductors and between each phase conductor and ground, each conductor exhibits self-capacitance between itself and ground and mutual capacitance with regard to other conductors, as illustrated in Fig. 7.

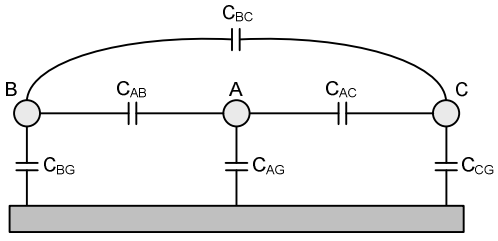

Fig. 7. The self- and mutual capacitances of a three-phase overhead line

Because we are ultimately interested in charging current, after each capacitance is derived from (2), the ac steady-state charging currents (I_{Ach}, I_{Bch}, and I_{Cch}) of a line or cable can be calculated per the following equation:

$$\begin{bmatrix} I_{Ach} \\ I_{Bch} \\ I_{Cch} \end{bmatrix} = j\omega \begin{bmatrix} C_{AA} & -C_{AB} & -C_{AC} \\ -C_{BA} & C_{BB} & -C_{BC} \\ -C_{CA} & -C_{CB} & C_{CC} \end{bmatrix} \begin{bmatrix} V_{A\_ave} \\ V_{B\_ave} \\ V_{C\_ave} \end{bmatrix} \quad (3)$$

where:

$C_{AA} = C_{AG} + C_{AB} + C_{AC}$

$C_{BB} = C_{BG} + C_{AB} + C_{BC}$

$C_{CC} = C_{CG} + C_{BC} + C_{AC}$

C_{AB}, C_{AC}, and C_{BC} = mutual capacitance in positive value.

For simplification, the ground wires are not shown in Fig. 7. With the addition of ground wires, the calculations of self- and mutual capacitances will be slightly adjusted.

For protection engineers, the positive-sequence and zero-sequence shunt capacitance or reactance is usually needed to calculate the steady-state charging current. For an ideally transposed line or cable, the sequence component of shunt capacitance can be calculated by (4) and (5).

$$C_{pos} = C_{self} - C_{mutual} = \frac{\left(C_{AA} + C_{BB} + C_{CC} + C_{AB} + C_{AC} + C_{BC}\right)}{3} \quad (4)$$

$$C_{zero} = C_{self} + 2C_{mutual} = \frac{\left(C_{AA} + C_{BB} + C_{CC} - 2C_{AB} - 2C_{AC} - 2C_{BC}\right)}{3} \quad (5)$$

C_{mutual} here is the mutual capacitance between phase conductors in negative value. From the appendix, the following formula can be used to obtain the approximate positive-sequence shunt reactance of the line:

$$C_{pos} = \frac{2\pi\varepsilon}{\ln \frac{d_m}{r_{eq}}} \quad (6)$$

where:

$d_m = \sqrt[3]{d_{AB} \bullet d_{AC} \bullet d_{BC}}$ and is the geometric mean distance among the three phases.

$r_{eq} = \sqrt[n]{n \bullet r \bullet R^{n-1}}$ and is the equivalent radius for an *n*-subconductor bundle.

r = the radius of the subconductor.

R = the radius of the bundle.

The zero-sequence shunt reactance can be approximated by the following:

$$C_{zero} = \frac{2\pi\varepsilon}{\ln \frac{(2h_m)^3}{r_{eq} d_m^2}} \quad (7)$$

where:

$h_m = \sqrt[3]{h_A h_B h_C}$ and is the geometric mean height of the line on the tower.

The positive-sequence charging current is calculated as:

$$I_{1ch} = j\omega C_1 \frac{V_{Ph-Ph}}{\sqrt{3}} \quad (8)$$

B. Impact of Line Transposition

The transposition of a transmission line is the practice of physically rotating the position of each phase conductor over the length of the line such that each conductor occupies each position for one-third of the total line length, as shown in Fig. 8.

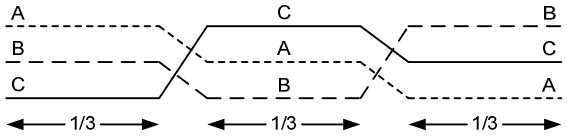

Fig. 8. Transposed transmission line

We can calculate the capacitance matrix for a 100-mile 345 kV line with the line geometry of Fig. 7. We assume a bundle of two 1,590 aluminum conductor steel-reinforced (ACSR) conductors (radius = 0.219 inches) separated by 18 inches. Spacing between phases is 15 feet, and the height of the three conductors is 120 feet. We ignore the sag and also the ground conductors. These simplifications have only a small impact on the result. For this exercise, we use a line constants program to determine the impedance components of the line. The resulting capacitance matrix is as follows:

$$C = \begin{bmatrix} 17.91 & -5.81 & -5.81 \\ -5.81 & 16.79 & -2.83 \\ -5.81 & -2.83 & 16.79 \end{bmatrix} \frac{nF}{mi} \quad (9)$$

Note that the B-phase and C-phase self-capacitances are equal and lower than that of A-phase, as suggested by the line geometry. The AB and AC mutual values are also equal and larger than BC.

Assuming a line length of 100 miles and applying (3), we obtain the following:

$$\begin{bmatrix} I_{Ach} \\ I_{Bch} \\ I_{Cch} \end{bmatrix} = \begin{bmatrix} 178.1j \\ 127.6 - 96.0j \\ -127.6 - 96.0j \end{bmatrix} A \quad (10)$$

The resulting positive-, negative-, and zero-sequence current magnitudes are 165 A, 18 A, and 4.6 A, respectively. Note that although the line is untransposed, the negative- and zero-sequence currents are quite small in comparison with the phase values.

We can calculate a transposed capacitance matrix based on the rotations shown in Fig. 8. On a line that is fully transposed, the resulting self- and mutual admittances are equal and can be calculated as $(C_{AA} + C_{BB} + C_{CC})/3$ = 17.16 nF per mile and $(C_{AB} + C_{BC} + C_{CA})/3$ = 4.82 nF per mile.

$$C_{TRANSPOSED} = \begin{bmatrix} 17.16 & -4.82 & -4.82 \\ -4.82 & 17.16 & -4.82 \\ -4.82 & -4.82 & 17.16 \end{bmatrix} \frac{nF}{mi} \quad (11)$$

The resulting positive-, negative-, and zero-sequence current magnitudes become 165 A, 0 A, and 0 A, respectively. The positive-sequence current is unchanged. The zero value of the negative- and zero-sequence charging currents is a result of perfectly balanced three-phase currents due to the symmetry of the capacitance matrix (assuming no major physical differences between the three line sections) and under the assumption that three-phase voltages are balanced.

It is important to note that a significant cost is incurred in the construction of transposition structures. The right of way may require more space. In addition, the possibility of electrical faults is often greater at the transposition locations. For these reasons, transposed lines are not at all common in many power systems.

C. Line and Cable Examples

Table I presents the shunt capacitance and charging currents of three example circuits: a 345 kV cable, a 345 kV overhead line (OHL), and a 765 kV overhead line. The cable and line data are provided in the appendix of this paper. The capacitances are calculated by using the Alternative Transients Program (ATP) JMarti model and the ATPDraw 5.6 line-check tool. The charging currents are calculated per nominal voltage of the line. From these examples, the charging current of a 5-mile cable is equivalent to that of a 100-mile overhead line with the same voltage level. Table I also shows that charging current is quite significant for long-distance extra-high-voltage (EHV) lines.

TABLE I
SHUNT CAPACITANCE AND CHARGING CURRENTS FOR SELECTED CIRCUITS

	Length	Shunt C_1 (at 60 Hz)	Shunt C_0 (at 60 Hz)	Charging Current
345 kV Cable	5 miles	1.9341 µF	1.0468 µF	145.2 A
345 kV OHL	100 miles	2.1363 µF	0.9892 µF	160.48 A
765 kV OHL	150 miles	2.9604 µF	1.9889 µF	492.9 A

III. IMPACT OF CHARGING CURRENT ON PROTECTION

We now can examine the impact of charging current on various line protection relays or elements. The analysis is performed for both steady-state and transient conditions. We used the Real Time Digital Simulator (RTDS®) to aid the analysis and model a 150-mile 765 kV line, as shown in Fig. 9. The 765 kV line data are given in the appendix. The CT ratio for line protection is 3000/5. To evaluate the charging current under the worst scenarios, the shunt reactor breakers were open in a number of simulation cases.

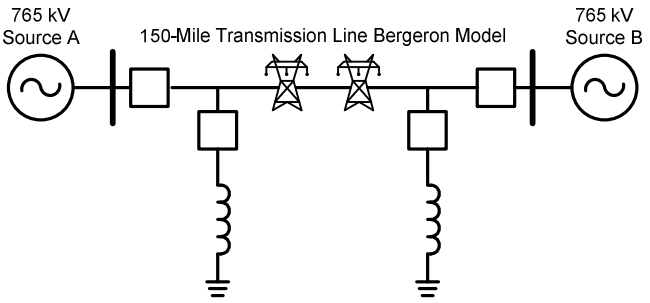

Fig. 9. A transmission line modeled on the RTDS

A. Steady-State Operation

In the sample system in Fig. 9, the 765 kV line is rated to carry 3,000 A of load current. In the steady state, this line draws about 600 A of charging current, which is about 20 percent of the CT primary rating with all shunt reactors out of service. Shunt current is elevated due to the Ferranti effect. If this EHV line is carrying enough load current, misoperation of a sensitive protection element due to charging current is unlikely because load current will dominate for line protection. The most challenging scenario is when the breaker is closed at only one end to energize the line. With only the charging current under such a condition, we can investigate to see if a particular operating characteristic might have a lower security margin. The operating points of the distance element, directional element, and line current differential (percentage differential and Alpha Plane) element are mapped into their respective operating characteristic presented in this subsection.

Fig. 10 plots the apparent impedances ($\vec{Z} = \vec{V} / \vec{I}$) against the mho distance element characteristics. It is evident that the cluster of apparent impedance is in the opposite quadrant of the complex plane, far away from the mho circles. Thus the distance element is not in danger of misoperation under steady-state conditions.

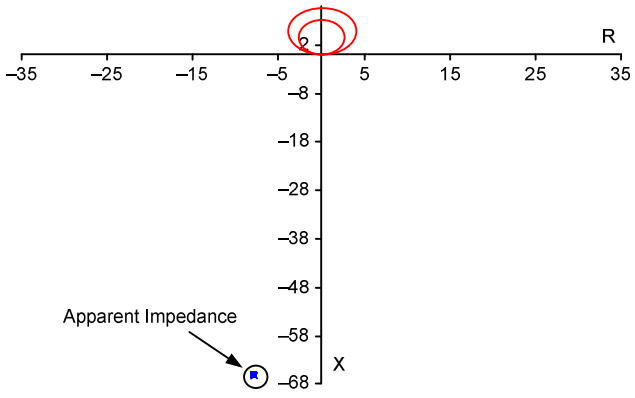

Fig. 10. Apparent impedance plot on distance element characteristic with standing charging current

A directional element can be developed in a variety of ways. Our analysis takes a generic approach, using 3I2 as the operating quantity and comparing its angle with the negated 3V2.

It can be seen from Fig. 11 that the angle difference between the polarizing quantity and operating quantity sits at about 90 degrees, which is obvious due to the shunt capacitance. But this would allow the directional element to assert the forward fault direction and operate if the magnitude of 3I2 or 3I0 is higher than the pickup setting (which may be set sensitively to cover a high-resistive ground fault). Because the directional overcurrent elements are the building blocks of pilot schemes, such as directional comparison blocking (DCB) or permissive overreaching transfer trip (POTT), the pilot scheme may misoperate when energizing the line or cable.

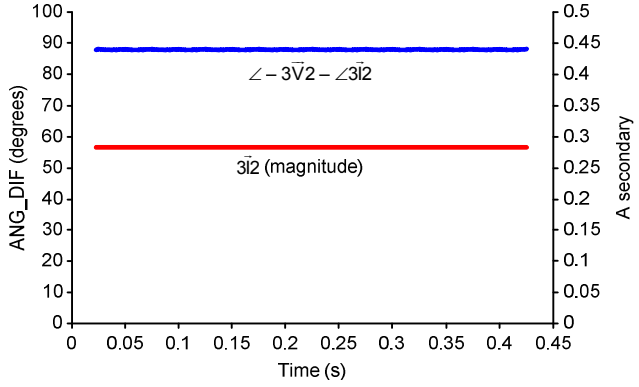

Fig. 11. Magnitude of negative-sequence current (3I2) and angle difference between 3V2 and 3I2 with standing charging current

Assume that the line is protected by a percentage differential (87L) element that has a pickup setting of 10 percent (0.1 per unit [pu] or 300 A primary). This 87L element also has a slope setting of 25 percent. The same settings apply to both phase currents and negative-sequence current, as shown in Fig. 12. Under a single-end feed situation, the magnitudes of the differential and restraint currents are equal. Therefore, whether the element will operate or not is solely dependent on the magnitude of the differential current and pickup setting.

The geometry of the overhead line conductors is, in general, symmetrical. Naturally, the phase charging current is much more prominent than the sequence charging current. In this case, the phase differential current has a magnitude of almost twice the pickup setting, while the negative-sequence current is about half of the pickup setting, as can be seen in Fig. 12. Therefore, the phase element is not secure if a sensitive pickup setting is applied. The degree of line asymmetry determines the security margin of the negative-sequence element.

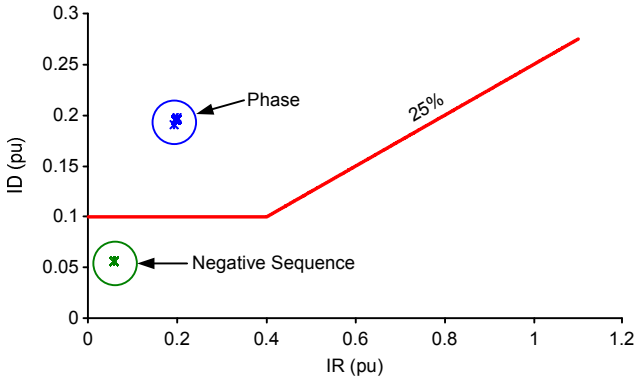

Fig. 12. Comparison of phase and negative-sequence percentage differential elements with standing charging current

Differential relays that use the Alpha Plane will check that the magnitude of the differential current is above the pickup setting and that the complex ratio k lies in the operate region of the Alpha Plane, as shown in Fig. 13.

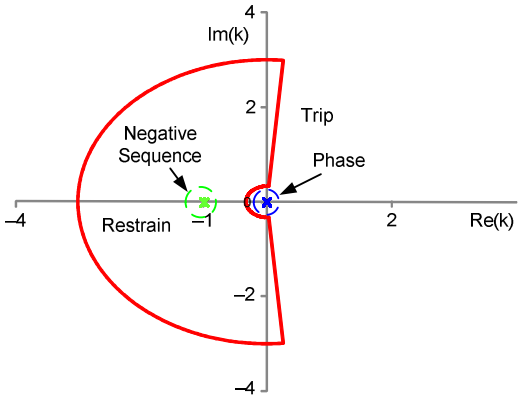

Fig. 13. Comparison of phase and negative-sequence differential elements on the Alpha Plane characteristic with standing charging current

The outcome of mapping the local and remote current phasors to the Alpha Plane characteristic is similar to that of the percentage differential characteristic. With the current from one line end being zero, the complex ratio k is either infinity or at the origin, which is always within the trip region of the Alpha Plane characteristic. Assuming the pickup setting is also 0.1 pu for the phase and negative-sequence elements, similarly, the phase differential current magnitude surpasses the pickup threshold, which leads to a trip decision. The negative-sequence element is secure, owing to the low steady-state value of the negative-sequence charging current.

B. Transient Operation

The existence of charging current in conjunction with certain power system transients poses a threat to line protection elements. Typically, the charging current appears with a higher magnitude during transients than at steady state.

This subsection covers the behavior of charging current during three different power system transients: line energization, external fault, and single-pole open (SPO).

1) Line Energization

When a circuit breaker (CB) closes to energize a line, the line capacitance (C_L) draws inrush charging current in the first few cycles. As illustrated in Fig. 14, this phenomenon can be understood as a resonance of the source plus the line reactance ($L_S + L_L$) against the line capacitance (C_L), which is damped by the resistance ($R_S + R_L$) in this RLC circuit. The natural frequency of this LC resonance is:

$$f_n = \frac{1}{2\pi\sqrt{(L_S + L_L) \cdot C_L}} \tag{12}$$

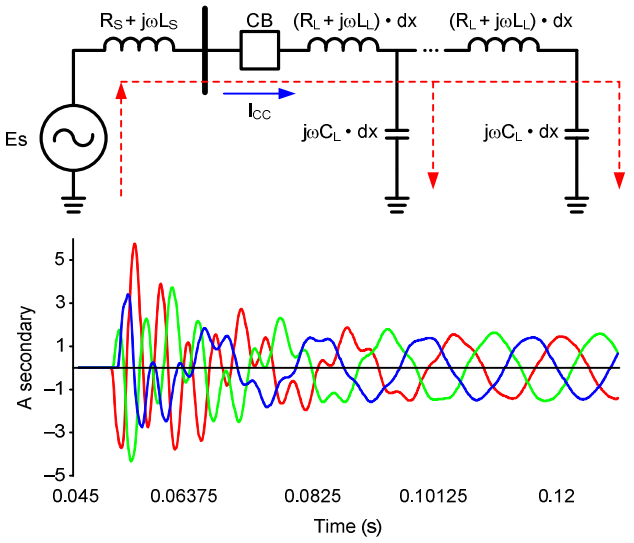

Fig. 14. Line energization, resonance, and inrush charging current

Because the serial line inductive reactance is much smaller than the shunt capacitance reactance, this initial resonance contains an abundance of high-frequency components. For the 765 kV line in Fig. 9, the frequency components in the inrush charging current are predominately in the neighborhood of the third harmonic (170 Hz). As the high-frequency content decays over time, the charging current waveform becomes more sinusoidal at the fundamental frequency.

In [3], the oscillation of the distance measurement was observed and the authors claimed such oscillation can cause distance protection to overreach or operate slowly. However, throughout our RTDS study with the 765 kV system in Fig. 9, there was no distance relay misoperation for either internal or external faults. It is recognized that different distance relays have different filters and different algorithms to compute phasors as well as impedance reach. The relays used in our RTDS tests are based on low-pass filters and cosine filters, which can effectively remove the high-frequency content in the transient. However, it was observed that there was some potential risk during the energization of the line. Fig. 15 shows the impedance loci when the line was energized; it can be seen that the apparent impedance moved erratically before eventually settling at the steady-state operating point (65∠–84°). The trace of apparent impedances appears to swiftly cross both Zone 1 and Zone 2 mho circles. However, the calculated impedance points all fell outside of both mho circles. It may be possible for Zone 1 distance elements to be armed for a short period of time if the CB closing takes place at a different point on the wave (POW). However, modern distance relays typically have multiple security measures that can prevent misoperation caused by transients. It is unlikely that Distance Zone 1 will simply trip by such types of transients.

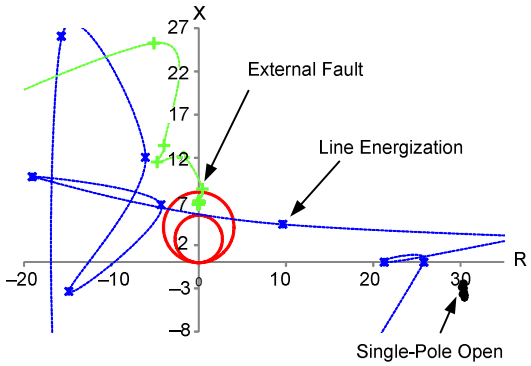

Fig. 15. Distance element response to power system transients

The directional element can be adversely affected by charging current during line energization. Fig. 16 shows the angle difference of negative-sequence voltage and current and the magnitude of negative-sequence current. For EHV lines, three single-pole breakers are typically applied. When the CB closes, the three poles may not be closed at exactly the same instant. Due to the combination of unequal pole closing and nonfundamental components in the inrush charging current, the polarizing quantity (3V2) and operating quantity (3I2) developed a series of angle difference values going in and out of the forward region (between the two horizontal green lines) multiple times in the test case. The highest negative-sequence magnitude is almost three times that at steady state, but it lasted just for a very short moment. Under the worst scenario, the directional overcurrent could assert forward fault momentarily, which means risk of misoperation for pilot schemes such as DCB or POTT. The coordination delay of such pilot schemes may be able to override such momentary directional overcurrent pickup, but it would be more secure to use a higher pickup setting or slightly longer time-delay settings to handle such transients caused by charging current at line energization in this example.

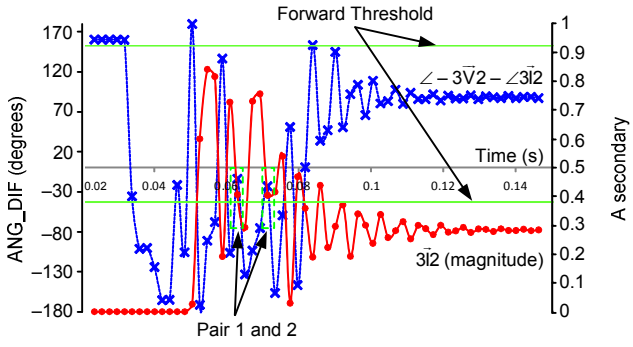

Fig. 16. Negative-sequence directional element during line energization

The negative-sequence percentage differential (87LQ) element was proven to be secure in steady state. In the event of line energization, the 87LQ element can be affected by unequal pole closing. In the RTDS case study, the A-phase took the lead to close first. Approximately 0.23 milliseconds later, the B-phase followed the A-phase and closed. The C-phase pole conducted after another 0.92-millisecond delay. The results are plotted in Fig. 17. The discrepancy of the pole closing time, coupled with differences in the phase filtering transients, results in negative-sequence current. In this study, the pickup of 0.1 pu guaranteed safe operation in steady states. But it was not enough to prevent the misoperation of 87LQ unless the pickup setting was doubled, or even tripled, temporarily for the line energization.

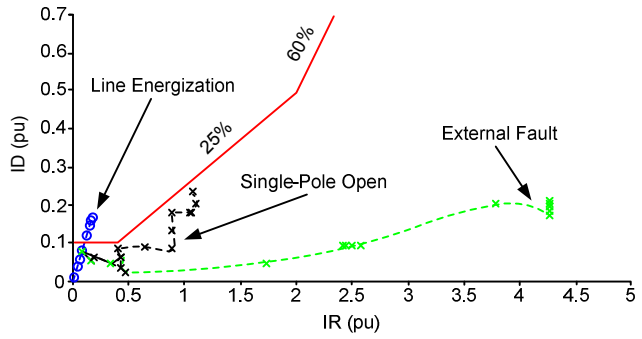

Fig. 17. Percentage differential element response to power system transients

Because the operating quantity is also the restraint quantity during line energization, the Alpha Plane-based 87LQ element is equally vulnerable to the elevated level of negative-sequence current due to unequal pole closing. Fig. 18 shows that the Alpha Plane 87LQ element would also trip for this case. A higher 87LQ pickup setting or temporary increase of pickup setting can help the relay to ride through the line energization, which means compromise on the sensitivity of the 87LQ element. However, this may not be a problem if the zero-sequence current differential element is used in parallel to provide coverage for a high-resistive ground fault.

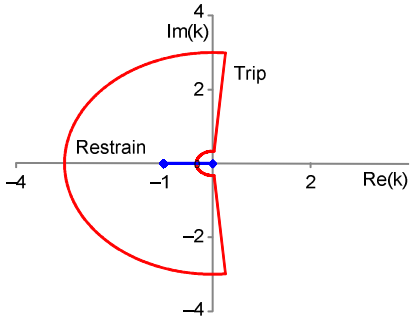

Fig. 18. Trajectory of *k* (negative sequence) superimposed onto the Alpha Plane characteristic during line energization

2) External Fault

An external fault is any system fault that is located outside the predefined zone of protection. A typical signature of an external fault is high fault current rushing through the protection zone. Some protection can be affected by the transients or CT saturation incurred by an external fault. A protective relay must be restrained for a fault adjacent to its protection zone in order for other relays designated to protect that part of the system to interrupt the fault, resulting in smaller system impact.

A B-phase-to-C-phase fault on Bus B was simulated on the sample system. The green trace in Fig. 15 represents the apparent impedance seen by the distance relay at Station A. It enters the Zone 2 mho circle and oscillates within an area close to the positive-sequence line impedance. It is obvious that the Zone 1 distance element is not in danger. The case study shows that the charging current does not affect the distance element, other than causing a small oscillation in the measured impedance values.

For the same case, the negative-sequence fault current seen by the relay at Station A is considerably larger than the charging current. The magnitude of the fault current shown in Fig. 19 is almost 30 times that of the charging current, which is understandable for a bus fault. This eliminates the impact of charging current in this case. Going into the fault, the angle difference between $-3\bar{V}2$ and $3\bar{I}2$ bounced for a short period of time because of transients. Then it quickly moved back into the forward region as soon as the magnitude of the operating quantity shot above the pickup threshold. The forward indication from this relay is correct. The response of the relay at Station B was recorded and analyzed as well; the fault in reverse direction asserted correctly.

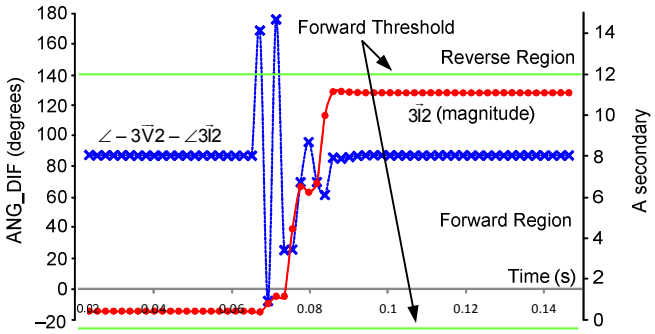

Fig. 19. Exposing negative-sequence directional element to an external fault

For exactly the same reason, neither the percentage differential element nor the Alpha Plane differential element (see Fig. 17 and Fig. 20) was triggered for this external fault, which also caused mild CT saturation. In a case of asymmetrical CT saturation (i.e., only one among all the CTs saturates heavily), the relay response to an external fault looked like that of a single-end feed condition. Proper relay design, such as an external fault detector, can prevent the differential relay from misoperating due to CT saturation. However, this is not related to charging current.

In Fig. 17, the restraint differential pair travels to the far right side of the percentage differential characteristic following the fault inception and stays well within the restraining region. The ratio of local over remote current phasor also sits in the vicinity of the ideal blocking point, as shown in Fig. 20.

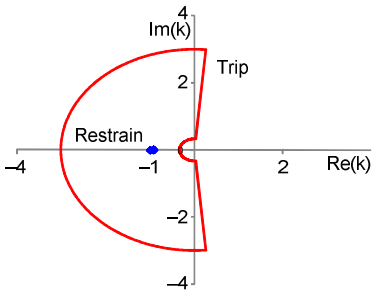

Fig. 20. Trajectory of *k* (negative sequence) superimposed onto the Alpha Plane characteristic when exposed to an external fault

Some relays are based on the phase angle comparison principle to use local and remote information with limited channel bandwidth. Fig. 21 plots the equivalent angle difference in electrical degrees, reflecting the time difference between the local current positive zero crossing and that of the remote current. Owing to the load current, the angle difference hovers around –150 degrees prior to the fault. If the line carries a very light load, the angle comparison can make a trip decision because both the local and remote currents are mainly composed of charging current. This can cause trouble for the phase angle comparison element if no additional check is available.

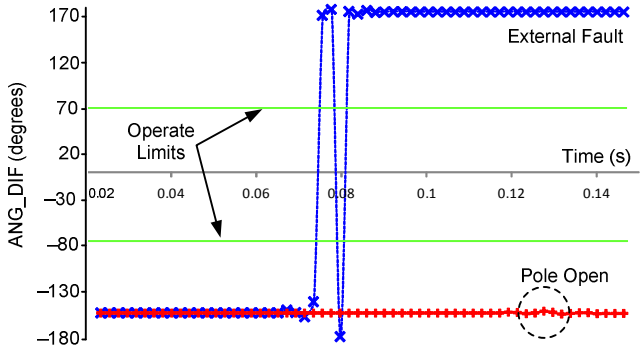

Fig. 21. Phase angle comparison element response to power system transients

When a fault occurs, the angle difference leaves its initial value and jumps to the opposite side of the trip region. The large through-fault current increases the angle difference between the local and remote currents, approaching the 180-degree theoretical limit, which prevents the relay from tripping. The conclusion is that charging current does not affect the phase comparison relay in the event of an external fault.

3) Single-Pole Open

Single-pole tripping of transmission lines is sometimes applied in order to improve system stability. To complete the single-pole tripping and reclosing cycle successfully, a protection element must remain secure during the pole-open time. Undesired operation from a protective relay when exposed to an SPO condition will inadvertently convert a single-pole tripping action to a three-pole tripping event. Once all three poles of the circuit breaker are open, the capacity to transmit power between the equivalent systems at either end of the line is reduced, thereby increasing the potential for system instability.

The B-phase-to-C-phase distance element was evaluated and is shown in Fig. 15. The cluster of apparent impedances seen by this element hardly moved from before and after pole open. It can be concluded that the mho distance element is not at serious risk of tripping from charging current under an SPO condition.

Next, we consider directional element behavior during an SPO condition. When one phase is open, the negative-sequence current is the result of both the unbalanced load and charging current. In Fig. 22, the angle difference between the operating and polarizing quantities leaves the forward region and enters the reverse region as the magnitude of $3\bar{I}2$ increases from 0.4 to 2.7 A due to the SPO condition. Without charging current, the negative-sequence current phasor leads the negated negative-sequence voltage phasor by about 166 degrees (Fig. 23). The presence of charging current pulls the operating quantity towards the forward region. Nevertheless, as can be seen from Fig. 22, this effect does not change the decision from the directional element because the load current has a much higher magnitude than the charging current.

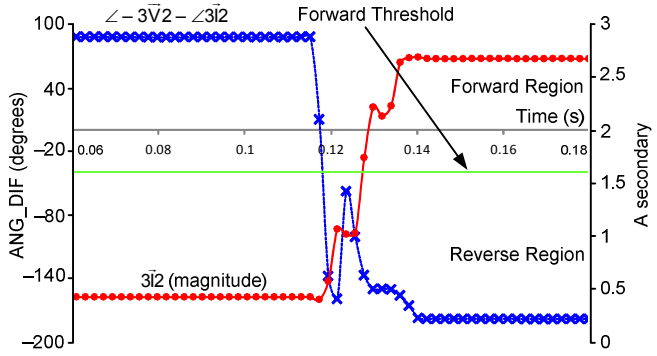

Fig. 22. Impact of SPO on the negative-sequence directional element

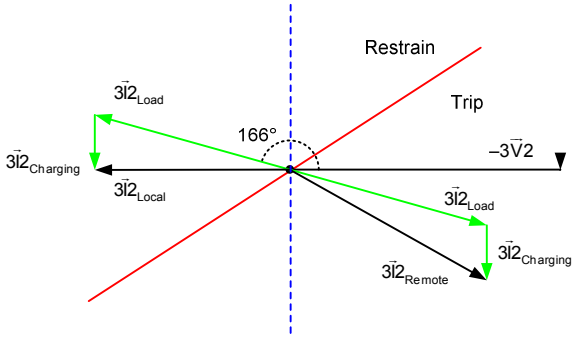

Fig. 23. Phasor diagram showing the relationship between 3V2 and 3I2 at the local and remote ends during an SPO condition

At the other end of the line, the direction of load flow creates an operating quantity in the forward region. The charging current moves the remote negative-sequence current closer to the forward direction maximum torque line. The forward-looking directional overcurrent element could operate. This justifies the need of inhibiting the sequence directional element during the period of pole open if the charging current is significant.

On the percentage differential plane, the main source of the negative-sequence differential current switches from the asymmetrical conductor placement to the absence of charging current contribution from the opened phase. Its magnitude grows approximately five times in this particular application. The trajectory of the restraint differential pair gets fairly close to the operating boundary in both the transient and steady state (refer to Fig. 17). Should the slope setting be more sensitive, the charging current may cause the operating point to enter into the tripping zone.

Fig. 24 illustrates similar results on the Alpha Plane characteristic. The elevated differential current drives the complex ratio *k* away from the ideal blocking point, making this element less secure. If the charging current has a higher magnitude compared with the load current, the security of the Alpha Plane element is at risk.

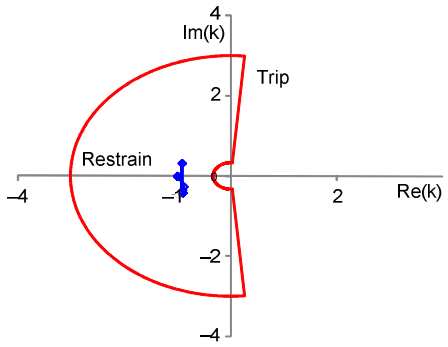

Fig. 24. Impact of SPO and charging current on the trajectory of *k* (negative sequence) superimposed onto the Alpha Plane characteristic

Typically, the phase angle comparison scheme operates on phase quantities. From the per-phase point of view, the relationship between the load current and charging current does not change because of the SPO condition. There is only a 2-degree shift in angle difference (0.1 milliseconds in coincidence time) between the local and remote current (see Fig. 21).

IV. Methods of Charging Current Compensation

From the previous simulations and analysis, we can see that the major impact of charging current is on differential (87L) relays. Directional overcurrent can also be affected under specific conditions. With a focus on 87L relays, this section presents a few solutions to handle the large charging current of long EHV lines or cables.

A. Setting Desensitization

Setting desensitization is the practice of accounting for charging current during the development of settings for the application. In the case of line current differential elements (both percentage differential and Alpha Plane), the setting procedure should begin with an assessment of the line charging current for the particular application. The pickup setting must be set at a safe margin above the charging current during line pickup to ensure security. Once the pickup setting is chosen, a calculation should be carried out to determine resistive fault coverage under worst-case circuit loading. In many applications, it is likely that the differential can be safely desensitized while still providing good resistive fault coverage.

Dynamic desensitization is a process of automatic adjustment of the protection element characteristics. It can take the form of logic implemented in the relay by the manufacturer or user-programmed logic or settings groups. These schemes adjust the sensitivity of the element during specific conditions when the charging current is known to be at a high level.

For instance, one dynamic desensitization scheme introduces a 1.5-cycle delay time into the trip path and doubles the differential pickup setting when any terminal is open. This state remains in effect for 3 cycles after the terminal closes in order to preserve security during energization inrush. This alleviates the need to consider inrush during the setting calculation process. One disadvantage of the approach is that it can create additional dependencies (e.g., circuit breaker auxiliary contacts). A second obvious disadvantage is that sensitivity is compromised for a fault that coincides with a desensitization condition.

B. Self-Compensation

There is no formal name for this next charging compensation method, so we refer to it as self-compensation because this method uses the differential current to compensate the differential current itself [4]. During normal operating conditions, the 87L relay takes the average differential current measured during the last few cycles as the charging current magnitude and subtracts it from the presently measured differential current. If a disturbance is detected, the updating of the prefault differential currents freezes and resumes after the normal operating condition is reestablished.

Because the differential current is continuously updated by subtracting the measured charging current, the operating quantity of such an 87L scheme is zero, or near zero, under steady state, no matter how high the charging current is. In the same way, the false differential current that can be caused by a CT error, a communications channel problem, tap load, or other reasons is treated as charging current to be compensated. It is a desirable feature of this method to have zero differential current under normal conditions because this allows more sensitive 87L settings for high-resistive internal faults. Compared with voltage-based charging compensation, this method can avoid voltage signals and line capacitance settings in the 87L scheme. If a shunt reactor is installed for the line, such an 87L relay in steady state will also be immune to the variations of charging current when the shunt reactor is put into or taken out of service once the relay adapts to the new false differential current level.

On one hand, this compensation method helps to increase 87L sensitivity. On the other hand, it may introduce extra differential current under an external fault condition. For an external fault, the voltage will be suppressed and the actual charging current will be less than that at prefault condition. Because the prefault differential current is taken as charging current, the compensation process will result in false differential current. The increased restraint currents or external

fault detector can help to prevent the 87L operation, but it is prudent to evaluate the 87L characteristic settings for some EHV lines, cables, or tap-load applications.

Another concern about this compensation method is that during the line or cable energization process, the method cannot provide any charging compensation, simply because there is no current prior to energization. From Fig. 14, the transient current caused by line capacitance could be quite high during energization, so the relay using this method can misoperate if the 87L element is set for sensitivity. A possible solution is to increase the 87L settings temporarily before and during the energization, but this will compromise the line protection during the energization process. A similar weakness is exposed at the time of de-energization when the charging current suddenly disappears, but the relay still subtracts the memorized current from its operating quantity.

C. Voltage-Based Compensation

Some line differential relays can incorporate a voltage measurement for backup protection. When the voltage signal is available, the instantaneous charging current drawn by the line or cable can be calculated in real time by applying (2) from Section II. The calculated charging current is then subtracted from the operating quantity, such that the 87L relay can have greater sensitivity. The basis of (3) is that the transmission line can be modeled as a two-port component, as shown in Fig. 25. This representation is called the transmission line T model. A more accurate way of approximating a physical line is to use the PI model, where the line capacitance is split evenly at the two line terminals.

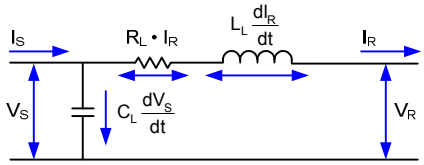

Fig. 25. Transmission line T model

Conversely, line current differential is no longer a current-only scheme if the voltage signal is involved in improving its performance. In the case of loss-of-potential (LOP) conditions, the voltage input from that phase is lost and so is the ability to carry out charging current compensation at that terminal. An enhancement employs the PI model method, which means that each of the two line terminals applies half of the total line capacitance in its charging current calculation. Under normal conditions, both terminals contribute to charging current compensation. If one terminal fails for any reason, the remaining healthy terminal takes up the responsibility to compensate for all the charging current. In addition to providing redundancy, including the voltages from both line ends in the algorithm also produces a more accurate result for compensation.

$$I_{ch} = \frac{C_L}{2} \bullet \frac{dV_S}{dt} + \frac{C_L}{2} \bullet \frac{dV_R}{dt} = C_L \bullet \frac{d\left(\frac{V_S + V_R}{2}\right)}{dt} \qquad (13)$$

From (13), the charging current is estimated based on the averaged line voltage. This approach has the advantage of working well when the voltage profile of the line is not flat.

In addition to LOP, the location of the potential transformer (PT) affects the availability of compensation. Assuming that the PT is placed on the bus side of the CB, the charging current compensation needs to be suspended if one phase of the CB is open. This is because the bus voltage does not follow the change in line voltage under SPO conditions. If it is still used to calculate the line charging current, the compensation can be inaccurate in a single-pole tripping application.

In order for multiple 87L relays to perform charging current compensation simultaneously, each relay in the scheme needs to know how many remote peers are also contributing. In any two-terminal application, this requirement is satisfied naturally because there must be a communications link between the local and remote relay. A bit in the data packet can be used to indicate if the sending relay is able to compensate.

A three-terminal line with a tap point in the middle brings more complexity to the design of a multiended charging current compensation scheme. As shown in Fig. 26, the communications channel between Relay X and Relay Z may be temporarily unavailable, which results in a three- terminal master-slave operation. Under such situations, these two relays are unable to perform differential calculations and are treated as slaves. Only Relay Y can perform 87L calculations because it has access to all the current information required to derive the differential and restraint quantities. It behaves as the master by commanding the slave relays to trip as soon as it sees a fault.

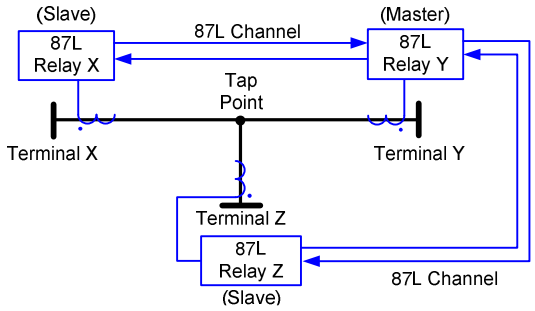

Fig. 26. Three-terminal master-slave operation

Because the slave relays cannot communicate with each other, neither can decide the portion of the line capacitance that it needs to compensate for. Consequently, the compensation algorithm has to be inhibited in slave relays. However, the master relay is capable of handling all of the charging current compensation for the 87L zone, albeit with reduced accuracy.

D. Other Compensation Methods

From [5] and [6], we know that the charging current can be handled by unconventional current differential schemes. In [5], the 87L relaying is built upon the calculated currents from a distributed line parameter model and the charging current is eliminated in the calculated currents.

For a uniformly distributed line, as shown in Fig. 27, it is well known that the voltage and current distributed along the line have the following relationship:

$$-\frac{\partial u}{\partial x} = r_0 i + l_0 \frac{\partial i}{\partial t} \tag{14}$$

$$-\frac{\partial i}{\partial x} = g_0 i + c_0 \frac{\partial u}{\partial t} \tag{15}$$

where:

r_0 = series resistance.

l_0 = series inductance.

g_0 = shunt conductance.

c_0 = shunt capacitance in unit length.

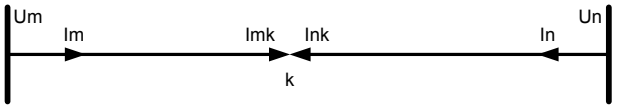

Fig. 27. Voltages and currents of an ultra-high voltage (UHV) line

From (14) and (15), the positive-sequence, negative-sequence, or zero-sequence currents at any point *k* on the line can be calculated by the following:

$$I_{mk\#} = I_{m\#}\, ch(\gamma_{\#} l_{mk}) - \frac{U_{m\#}}{Z_{c\#}} sh(\gamma_{\#} l_{mk}) \tag{16}$$

$$I_{nk\#} = I_{n\#} ch(\gamma_{\#} l_{nk}) - \frac{U_{n\#}}{Z_{c\#}} sh(\gamma_{\#} l_{nk}) \tag{17}$$

where:

sh( ) and ch( ) = hyperbolic functions.

Z_c = the line characteristic impedance.

γ = the propagation constant.

l_{xy} = the distance from point *x* to point *y* on the line.

The # symbols in (16) and (17) are replaced by 1, 2, or 0 for positive-, negative-, or zero-sequence currents. With sequence components, the three-phase currents at point *k* can be obtained as well. Using positive-sequence currents as an example, the differential current and restraint current of the 87L scheme are based on the calculated currents at a specific point *k* on the line:

$$I_{diff\_1} = \left| I_{mk1} + I_{nk1} \right| \tag{18}$$

$$I_{restraint\_1} = \left| I_{mk1} - I_{nk1} \right| \tag{19}$$

Because the 87L operating and restraint quantities are derived from the distributed line model per (14) through (17), the charging current is excluded naturally. As with conventional voltage-based compensation, this method also needs a voltage signal, but this method can take any point on the line to perform differential and restraint calculations, which can improve the sensitivity of the 87L scheme, according to [5]. From the simulation tests in [5], the proposed 87L relay can handle high-resistive faults and is secure for external faults. There are also recommendations in [5] on how to select the *k* point to optimize the sensitivity and dependability of the 87L relay.

Similarly, there are other 87L schemes that use calculated current-per-line modeling to eliminate the impact of charging current for UHV lines. Theoretically, such 87L schemes can provide alternative solutions to handle large charging current for UHV lines or cables, but the practical applications and operational experience of such 87L relays are not evident at this time.

V. Dynamic Analysis of the Voltage-Based Compensation Method

This section focuses on the performance of voltage-based compensation under the same system transients as those discussed in Section III. The T model and PI model method introduced in Section IV both belong to the model category of approximating the line with lumped parameters.

The accuracy of the lumped model degrades as the line length increases and so does the charging current calculated from such a model. A long line can be better approximated by connecting a number of T sections in series so that each T section represents a shorter distance. A continuation of this process brings out the distributed model, where the line is divided into an infinite number of T sections. This is also how the classic telegrapher's equations describe the current and voltage relationship of a transmission line.

Implementing a distributed model for charging current estimation in most digital relays would be a challenge. The lumped model works well at fundamental frequency. However, oscillations as a result of power system transients cause the line to draw charging current at higher frequencies. Depending on the line length, the line shunt capacitance modeled by a single T section might deviate from the lumped value at certain natural frequencies of the line. These resonant frequencies will be significantly larger than the fundamental if the line is relatively short (less than 100 miles). For lines of longer length (greater than 200 miles), the resonant frequencies will approach the fundamental.

Using the 765 kV line data from the appendix, the magnitude and angle of the shunt susceptance are plotted in Fig. 28. According to the lumped model, the line susceptance has a magnitude proportional to the system frequency and its angle is always at 90 degrees. In this case study, the lumped model offers an accurate representation until the system frequency goes above 120 Hz. As the frequency ramps up, the susceptance magnitude given by the distributed model is either higher or lower than that given by the lumped model, which is a straight line with a constant slope. In addition, the overall characteristic of the line shunt component shifts from being capacitive to being inductive at certain frequencies.

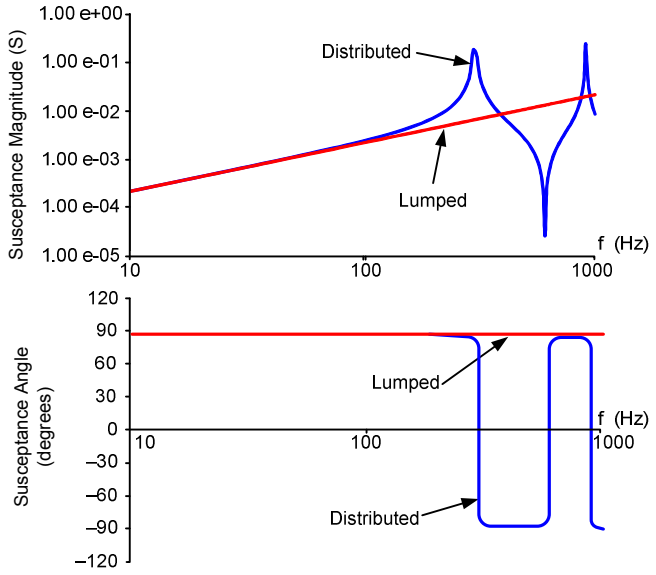

Fig. 28. Comparing the lumped and distributed line capacitance models

The theoretical analysis can be verified by the simulation results presented in the following subsections. These three transients have one thing in common: a temporary high-frequency surge in the first few cycles of the event.

A. Line Energization

The top half of Fig. 29 shows the charging current waveforms captured from a line energization case. The blue trace is the charging current from the RTDS simulation, which uses a distributed model. The red trace is the result of feeding the voltage signals to the lumped model. Due to the existence of high-frequency components at the initial stage of line energization, these two traces are slightly different. Once the transient subsides, the waveforms closely match.

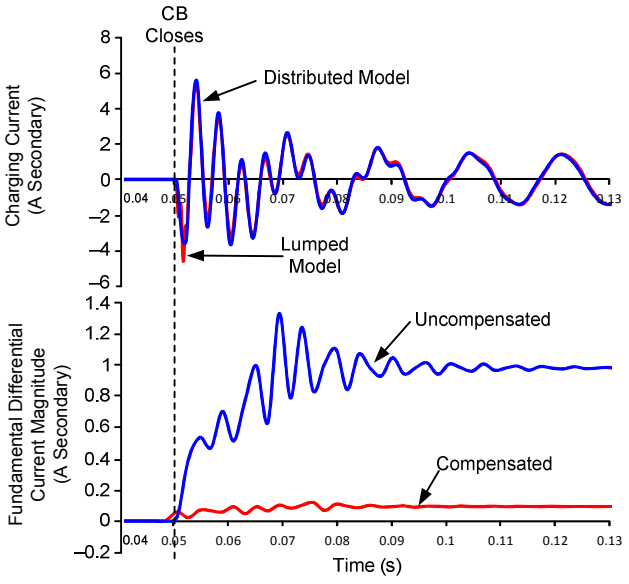

Fig. 29. Accuracy of charging current calculation during line energization transient

The 87L relay supplemented with voltage-based compensation calculates the charging current using the lumped parameters and subtracts this charging current from the differential signal. The calculated charging current is slightly different from the actual charging current, which can be accurately simulated by the distributed model. Therefore, the difference in the current produced by the distributed and the lumped models is in fact the differential current seen by the 87L element after the compensation. The lower half of Fig. 29 plots the fundamental magnitude of differential current with and without voltage-based compensation.

It is evident that the compensated differential current has a much smaller magnitude in comparison with that of the phase charging current, even during the transient when there is a mismatch between the distributed and the lumped models. With charging current compensation enabled, the differential current is reduced to less than 10 percent of its uncompensated value throughout the simulated event. Because most digital relays operate on only fundamental quantities, a sensitive pickup setting can be safely applied to the 87L element without concern about inrush charging current.

B. External Fault

When a low-impedance path is formed by a fault, the energy stored in line capacitance will be discharged into that fault point. Similar to the line energization transient, there is an initial RLC resonance between the shunt capacitance and series reactance. The ringing of charging current in Fig. 30 is clear evidence of this resonance.

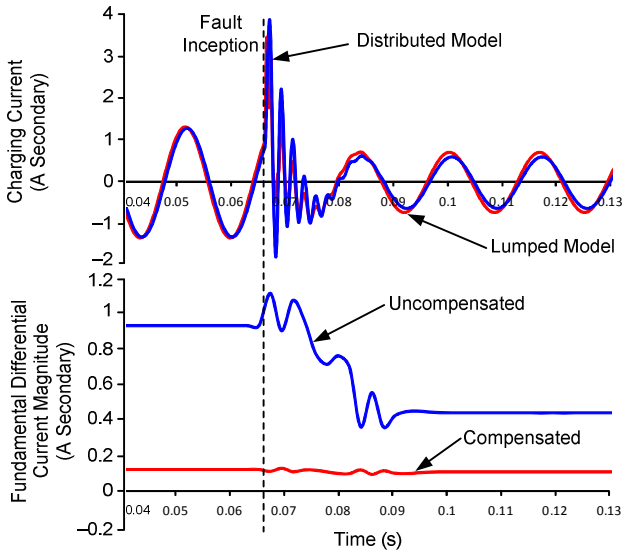

Fig. 30. Charging current compensation at the time of an external fault

There is a small difference between the behavior of the lumped model and the distributed model at the resonant frequency. However, the fundamental magnitude of the difference current is no higher than the prefault standing differential current, and with voltage-based compensation, it is much lower than that of the real charging current. In the steady state of an external fault, the averaged line voltage on the faulted phase is lower than nominal. The amount of charging current absorbed by the faulted phase is consequently lower.

C. Single-Pole Open

Assume the A-phase voltage drops to zero because of an A-phase-to-ground fault and secondary arcing can be ignored after the breaker interrupts the fault current. Prior to the fault, the B-phase charging current can be expressed as:

$$\overline{I_{Bch}} = j\omega C_{BG} \bullet \overline{V_{BG}} + j\omega C_{AB} \bullet \overline{V_{BA}} + j\omega C_{BC} \bullet \overline{V_{BC}} \qquad (20)$$

During the pole-open interval, $\overline{V_{BA}}$ is identical to $\overline{V_{BG}}$, considering that the faulty phase is grounded. This effect is visualized in Fig. 31.

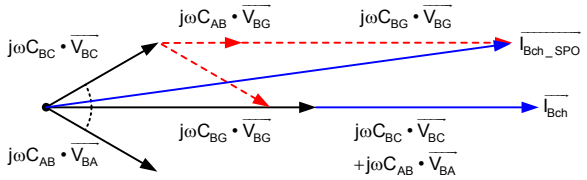

Fig. 31. Shift of charging current phasor due to SPO

$\overline{I_{Bch\_SPO}}$ represents the charging current phasor at the time when the breaker A-phase is open. It has a slightly smaller magnitude and advanced angle compared with $\overline{I_{Bch}}$. Regardless of the compensation method, misoperation due to such a small variation in charging current is unlikely.

Fig. 32 shows that the high-frequency discharge transient on the unfaulted phase lasts for about 2 cycles. To eliminate the impact of change in voltage on healthy phases before the fault clearing, the fault and pole-open events are simulated to occur at exactly the same time. The transition of B-phase and C-phase charging currents from their prefault values to their respective pole-open state values completes within the same time frame. The top oscillography in Fig. 32 proves the anticipated magnitude reduction and phase shift. The compensated differential current magnitude plotted in the lower half of Fig. 32 drops to 0.05 A once the transient comes to an end.

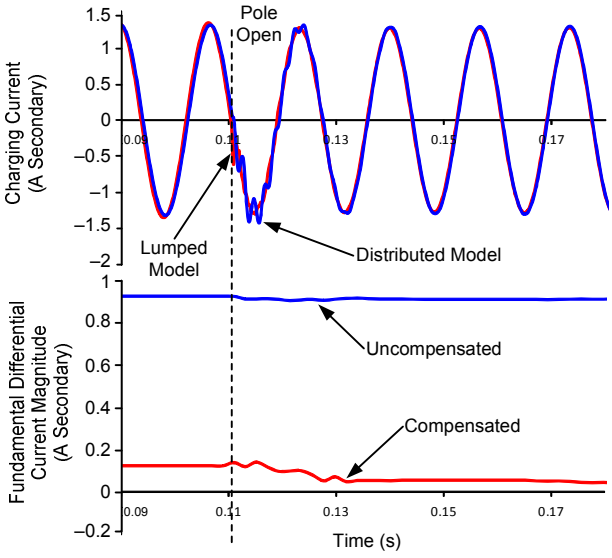

Fig. 32. Impact of SPO on line charging current

To conclude, the 87L element will not be stressed by any of these events as long as the voltage-based charging current compensation is active.

VI. Application Guidelines

Section II shows that charging current is mainly a concern for line current differential and phase comparison schemes. Indeed, these are the only types of relays for which manufacturers provide charging current compensation. In addition, sequence directional elements should be checked for line energization and pole-open operation. In this section, we provide guidelines for determining when to use charging current compensation for current differential applications.

A. General Guidelines

The first step in the process is determination of the charging current. Shunt capacitances can be calculated using (6) and (7) or using a line constants program. The difference between the results obtained by the two approaches is typically less than 10 percent. Charging current is then calculated using (8).

When charging current is significant, sequence directional elements can misoperate during line energization. In this case, consider either desensitizing the element or delaying operation when the line is energized. Sequence directional elements should be blocked by pole-open logic on lines that employ single-pole tripping.

The pickup setting of the phase differential element must be set higher than the value of the standing charging current. To ensure security during line energization, a margin of 200 percent can be considered. In relays that employ dynamic desensitization, a lower pickup setting margin (150 percent) can be chosen, depending on the particular implementation.

The second step checks the coverage provided for resistive faults during line loading. In general, the following equation gives the internal ground fault current for a two-terminal line [7]:

$$If_{PHG} = \frac{3 \bullet \left[V_{PHN} - I_{LOAD} \bullet \left(Z1S + d \bullet Z1L \right) \right]}{2\left(Z1S + d \bullet Z1L \right) \bullet C1 + \left(Z0S + d \bullet Z0L \right) \bullet C0 + 3 \bullet R_F} \qquad (21)$$

where:

$$C1 = \frac{Z1R + (1-d) \bullet Z1L}{Z1S + Z1L + Z1R}$$

$$C0 = \frac{Z0R + (1-d) \bullet Z0L}{Z0S + Z0L + Z0R}$$

Z1R, Z0R, Z1S, and Z0S = the positive- and zero-sequence source impedances.

Z1L and Z0L = the positive- and zero-sequence line impedances.

V_{PHN} = the line-to-neutral voltage.

d = the location of the fault (0 to 1).

R_F = the fault resistance.

The fault current should be checked for $d = 0$ and $d = 1$ for the highest fault resistance for which the phase elements need to operate. This value should be greater than the pickup setting chosen in the first step.

For an Alpha Plane element, the ratio K can be calculated as the following:

$$K_{PH} = \frac{2 \bullet (1 - C1) + (1 - C0) + 3 \bullet \frac{I_{LOAD}}{If_{PHG}}}{2 \bullet C1 + C0 - 3 \bullet \frac{I_{LOAD}}{If_{PHG}}} \quad (22)$$

Adequate coverage is verified by checking the magnitude and angle of K_{PH} against the ratio and blocking angle settings of the element.

For percentage differential, the restraint signal is the following:

$$I_R \approx \left| \frac{If_{PHG}}{2} + I_{LOAD} \right| \quad (23)$$

Adequate coverage is verified by checking that the differential current is greater than I_R multiplied by the slope setting.

Sequence differential elements applied on lines employing single-pole tripping and with significant charging current should either be desensitized or blocked by pole-open logic.

If the differential element cannot provide the needed fault coverage, then the use of line charging compensation is warranted. Relays that employ voltage-based compensation require that the positive- and zero-sequence capacitances (or susceptances) of the line be entered as a setting. Consequently, the differential elements can be set without having to consider charging current. However, because a voltage measurement is required, voltage-based compensation is impacted by LOP or fuse-failure events. Some relays have built-in logic that allows the user to fall back to more secure settings under LOP conditions. Other relays may not have built-in logic, but the same functionality may be achievable using programmable logic and settings groups. In either case, such schemes improve the availability of the differential protection but require additional effort in settings development. Relays that employ the self-compensation method described in Section IV benefit from reduced settings requirements but do not perform equally well.

When negative-sequence and zero-sequence elements are applied, an alternate strategy is to require the phase elements to be sensitive for only three-phase faults. The fault resistance requirements are lower for this fault type. As a result, more margin is available for setting the element. The sequence elements provide excellent resistive fault coverage, regardless of loading. Sequence charging currents are significantly lower, even on untransposed lines, as evidenced in Section II. The relaxed sensitivity requirement on the phase element lessens the need for charging current compensation.

B. Shunt Reactor Applications

Shunt reactors are often applied on long lines for voltage control (see Fig. 33). These reactors provide a portion of the line charging current. This creates an error in compensation provided by voltage-based schemes. One solution to the problem is to calculate the combined susceptance of the parallel inductive and capacitive branches and to use this value when setting the relay. However, there are several problems with this approach. The first problem is that the degree to which the capacitance of the line and the inductance of the reactors cancel will differ in the transient and steady states. As a consequence, capacitive inrush can still occur. The second problem is dealing with reactor switching. To achieve optimal compensation, different settings would need to be applied with the reactors in and out of service, and this can be impractical because changes need to be made to both local and remote relays.

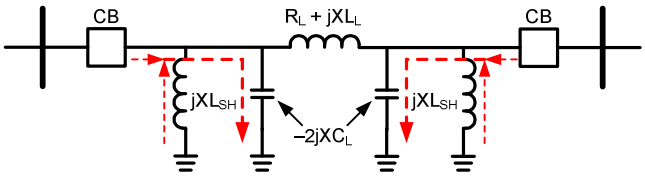

Fig. 33. Transmission line with shunt reactors showing the distribution of charging current

A better solution is to measure the contribution of the reactors to the zone, as shown in Fig. 34. Bringing the CT at a shunt reactor branch into the 87L scheme, the shunt reactor is excluded from the 87L protection zone. Now, the voltage-based compensation can use the full susceptance of the line as its setting once again. Reactor switching and line energization are no longer an issue.

The presence of a switched shunt reactor in the middle of the line presents challenges for either approach.

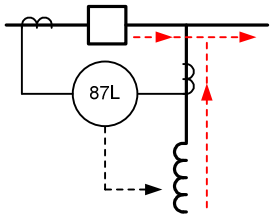

Fig. 34. Direct measurement of shunt reactor contribution

VII. Conclusion

This paper explores the impact of charging current on line protection elements through the use of a 765 kV line model.

Differential elements are more adversely impacted than other elements because they derive their operating signal from a summation of currents into the protected circuit and charging current is an unbalanced current entering the 87L zone.

Directional and differential elements that use negative- or zero-sequence components are at risk during line energization with unequal pole closing or under pole-open conditions with low load. These elements should either be set at a safe margin above the phase capacitive current or be supervised by an pole-open indication (assuming no charging current compensation).

The security of distance elements was practically unaffected during both steady-state and transient testing. Proper filtering ensures that the impact on the impedance measurement for internal faults is minimal. This was confirmed in our testing.

This paper also reviews schemes for line charging current compensation. Several schemes are evaluated practically. Each scheme has particular advantages and disadvantages. The voltage-based compensation scheme is analyzed during dynamic operation. Given that the requirement for a voltage measurement and additional settings is typically not onerous, the voltage-based compensation scheme provides good performance both in the steady state and during transients.

Application of charging current compensation is not always required. Often, the charging current can be accounted for through the appropriate application of settings.

VIII. Appendix

A. Circuit Parameters for Table I

The construction (see Fig. 35) and parameters for the 345 kV cable in Table I are the following:

- Conductor radius: 1.079 inches
- Sheath radius: 1.147 inches
- Total radius: 2.5 inches
- Resistivity of conductor: 1.7241 e-08 Ωm
- Resistivity of sheath: 2.14 e-07 Ωm
- Relative permittivity of insulation: 2.4
- Earth resistivity: 100 Ωm

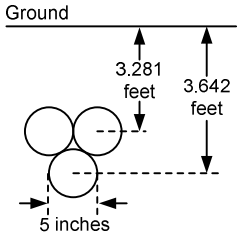

Fig. 35. 345 kV cable construction

The parameters for the 345 kV overhead line in Table I are the following:

- Number of subconductors per bundle: 2
- Subconductor radius: 0.772 inches
- Subconductor spacing: 18.0 inches
- Conductor dc resistivity: 0.028275 Ω per mile
- Horizontal distance between two bundles: 15 feet
- Height at tower: 120.0, 120.0, and 120.0 feet
- Sag at midspan: 28.0 feet
- Ground wire radius: 0.21875 inches
- Ground wire horizontal distance: 24 feet
- Ground wire height at tower: 145.0 and 145.0 feet
- Ground wire sag at midspan: 16.0 feet
- Ground wire dc resistivity: 0.646 Ω per mile

The parameters for the 765 kV overhead line in Table I are the following:

- Number of subconductors per bundle: 6
- Subconductor radius: 0.503 inches
- Subconductor spacing: 15.0 inches
- Conductor dc resistivity: 0.015817 Ω per mile
- Horizontal distance between two bundles: 45 feet
- Height at tower: 115.0, 115.0, and 115.0 feet
- Sag at midspan: 65.0 feet
- Ground wire radius: 0.323 inches
- Ground wire horizontal distance: 90 feet
- Ground wire height at tower: 155.0 and 155.0 feet
- Ground wire sag at midspan: 50.0 feet
- Ground wire dc resistivity: 0.646 Ω per mile

B. Capacitance of a Three-Phase Overhead Line

The method of images is shown in Fig. 36, where conductors with a negative charge are placed on the opposite side of the earth plane to create the effect of a zero-potential surface. The potential difference between the A-phase conductor and ground generated by the positive charge on itself and the negative charge carried by its mirrored image is:

$$V_{A\_SELF} = \int_{h_A}^{r_{eq}} \frac{q_a}{2\pi\varepsilon} \bullet \frac{dx}{x} + \int_{h_A}^{2h_A} \frac{-q_a}{2\pi\varepsilon} \bullet \frac{dx}{x}$$
$$= \frac{q_a}{2\pi\varepsilon} \ln \frac{h_A}{r_{eq}} - \frac{q_a}{2\pi\varepsilon} \ln \frac{h_A}{2h_A} \quad (24)$$

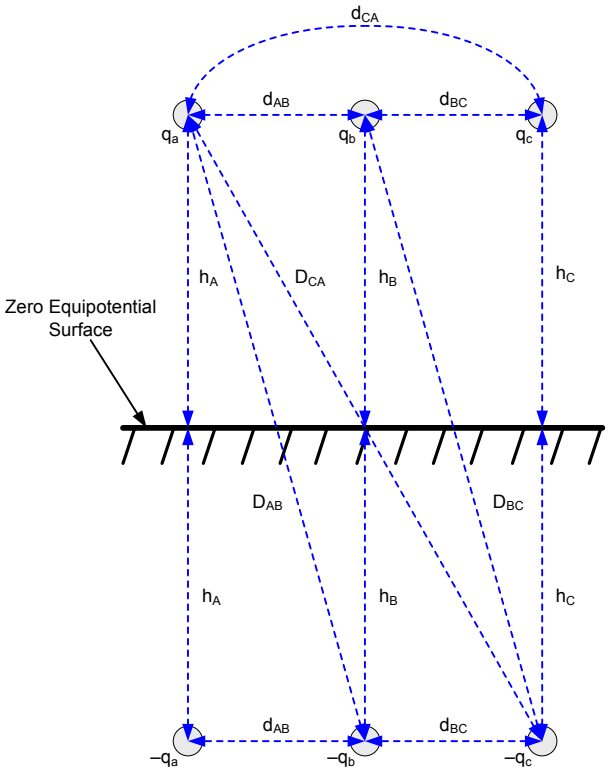

Fig. 36. Overhead line geometry

Likewise, the potential difference between the A-phase conductor and ground generated by the positive charge on the B-phase conductor and its negative image is:

$$V_{AB} = \int_{h_B}^{d_{AB}} \frac{q_b}{2\pi\varepsilon} \bullet \frac{dx}{x} + \int_{h_B}^{D_{AB}} \frac{-q_b}{2\pi\varepsilon} \bullet \frac{dx}{x} = \frac{q_b}{2\pi\varepsilon} \ln \frac{h_B}{d_{AB}} - \frac{q_b}{2\pi\varepsilon} \ln \frac{h_B}{D_{ab}} \quad (25)$$

The potential differences between the conductor and ground, when taking all three phases into account, are:

$$V_A = \frac{q_a}{2\pi\varepsilon} \ln \frac{2h_A}{r_{eq}} + \frac{q_b}{2\pi\varepsilon} \ln \frac{D_{AB}}{d_{AB}} + \frac{q_c}{2\pi\varepsilon} \ln \frac{D_{CA}}{d_{CA}} \quad (26)$$

$$V_B = \frac{q_a}{2\pi\varepsilon} \ln \frac{D_{AB}}{d_{AB}} + \frac{q_b}{2\pi\varepsilon} \ln \frac{2h_B}{r_{eq}} + \frac{q_c}{2\pi\varepsilon} \ln \frac{D_{BC}}{d_{BC}} \quad (27)$$

$$V_C = \frac{q_a}{2\pi\varepsilon} \ln \frac{D_{CA}}{d_{CA}} + \frac{q_b}{2\pi\varepsilon} \ln \frac{D_{BC}}{d_{BC}} + \frac{q_c}{2\pi\varepsilon} \ln \frac{2h_C}{r_{eq}} \quad (28)$$

In the zero-sequence capacitance calculation, assume that:

$$q_a = q_b = q_c = q_0 \quad (29)$$

$$3V_0 = V_a + V_b + V_c \quad (30)$$

The result of adding (26), (27), and (28) together is:

$$3V_0 = \frac{q_0}{2\pi\varepsilon} \ln \frac{2h_A \bullet 2h_B \bullet 2h_C}{r_{eq}^3} + \frac{q_0}{2\pi\varepsilon} \ln \frac{D_{AB}^2 \bullet D_{BC}^2 \bullet D_{CA}^2}{d_{AB}^2 \bullet d_{BC}^2 \bullet d_{CA}^2} = \frac{q_0}{2\pi\varepsilon} \ln \frac{(2h_m)^3}{r_{eq}^3} + \frac{q_0}{2\pi\varepsilon} \ln \frac{D_m^6}{d_m^6} \quad (31)$$

$$V_0 = \frac{q_0}{2\pi\varepsilon} \ln \frac{2h_m \bullet D_m^2}{r_{eq} \bullet d_m^2} \quad (32)$$

The tower height (h_m) is typically much greater than the distance between the phase conductors (d_m). Therefore, D_m can be approximated by $2h_m$, and (32) can be rewritten as:

$$V_0 = \frac{q_0}{2\pi\varepsilon} \ln \frac{(2h_m)^3}{r_{eq} \bullet d_m^2} \quad (33)$$

From (33), the zero-sequence line capacitance is:

$$C_0 = \frac{q_0}{V_0} = \frac{2\pi\varepsilon}{\ln \frac{(2h_m)^3}{r_{eq} \bullet d_m^2}} \quad (34)$$

When calculating the positive-sequence capacitance, the relationship turns into:

$$q_a = \alpha \bullet q_b = \alpha^2 \bullet q_c \quad (35)$$

$$3V_1 = V_a + \alpha \bullet V_b + \alpha^2 \bullet V_c \quad (36)$$

Substituting (26) through (28) for the phase voltages in (36) yields:

$$3V_1 = \frac{q_a}{2\pi\varepsilon} \ln \frac{2h_A \bullet 2h_B \bullet 2h_C}{r_{eq}^3} + \frac{\alpha \bullet q_a}{2\pi\varepsilon} \ln \frac{D_{AB} \bullet D_{BC} \bullet D_{CA}}{d_{AB} \bullet d_{BC} \bullet d_{CA}} + \frac{\alpha^2 \bullet q_a}{2\pi\varepsilon} \ln \frac{D_{AB} \bullet D_{BC} \bullet D_{CA}}{d_{AB} \bullet d_{BC} \bullet d_{CA}} = \frac{q_a}{2\pi\varepsilon} \ln \frac{(2h_m)^3}{r_{eq}^3} + \frac{(\alpha + \alpha^2) \bullet q_a}{2\pi\varepsilon} \ln \frac{D_m^3}{d_m^3} = \frac{q_a}{2\pi\varepsilon} \ln \frac{(2h_m)^3 \bullet d_m^3}{r_{eq}^3 \bullet D_m^3} \quad (37)$$

Because $D_m \approx 2h_m$, the above equation can be simplified to:

$$3V_1 = \frac{q_a}{2\pi\varepsilon} \ln \frac{d_m^3}{r_{eq}^3} \quad (38)$$

The positive-sequence line capacitance can thus be found as the following:

$$C_1 = \frac{2\pi\varepsilon}{\ln \frac{d_m}{r_{eq}}} \quad (39)$$

IX. References

[1] B. Kasztenny, I. Voloh, and E. A. Udren, "Rebirth of the Phase Comparison Line Protection Principle," proceedings of the 59th Annual Conference for Protective Relay Engineers, College Station, TX, April 2006.

[2] J. J. Grainger and W. D. Stevenson, Jr., *Power System Analysis*. McGraw-Hill, 1994.

[3] T. Kase, Y. Kurosawa, and H. Amo, "Charging Current Compensation for Distance Protection," *IEEE Power Engineering Society General Meeting*, Vol. 3, June 2005, pp. 2683–2688.

[4] Z. Gajic, I. Brncic, and F. Rios, "Multi-Terminal Line Differential Protection With Innovative Charging Current Compensation Algorithm," proceedings of the 10th IET International Conference on Developments in Power System Protection, Manchester, UK, March 2010.

[5] Z. Y. Xu, Z. Q. Du, L. Ran, Y. K. Wu, Q. X. Yang, and J. L. He, "A Current Differential Relay for a 1000-kV UHV Transmission Line," *IEEE Transactions on Power Delivery*, Vol. 22, Issue 3, July 2007, pp. 1392–1399.

[6] Y. Qiao and C. Qing, "An Improved Current Differential Protective Principle of UHV Transmission Line," proceedings of the Asia-Pacific Power and Energy Engineering Conference, Wuhan, China, March 2011.

[7] G. Benmouyal, "The Trajectories of Line Current Differential Faults in the Alpha Plane," proceedings of the 32nd Annual Western Protective Relay Conference, Spokane, WA, October 2005.

X. BIOGRAPHIES

Yiyan Xue received his B.Eng. from Zhejiang University in 1993 and M.Sc. from the University of Guelph in 2007. He is currently a Senior Engineer in the American Electric Power (AEP) P&C Standards Group, working on protection standards, relay settings, fault analysis, and simulation studies. Before joining AEP, he was an Application Engineer with GE Multilin to provide consulting services on relay settings, scheme design, and RTDS studies. Prior to GE, he had ten years with ABB working on P&C system design, commissioning of relays, and RTU systems. He is a senior member of IEEE and a Professional Engineer registered in Ohio.

Dale Finney received a bachelor of engineering degree from Lakehead University in 1988 and a master of engineering degree from the University of Toronto in 2002. He began his career with Ontario Hydro, where he worked as a protection and control engineer. Currently, Dale is employed as a senior power engineer with Schweitzer Engineering Laboratories, Inc. His areas of interest include generator protection, line protection, and substation automation. Dale holds several patents and has authored more than 20 papers in the area of power system protection. He is a member of the main committee of the IEEE PSRC, a member of the rotating machinery subcommittee, and a registered professional engineer in the province of Ontario, Canada.

Bin Le received his B.S.E.E. degree from Shanghai Jiao Tong University in 2006 and an M.S.E.E. degree from the University of Texas at Austin in 2008. He has been employed by Schweitzer Engineering Laboratories, Inc. since 2008. Bin currently holds the position of power engineer in the research and development division. He is a member of IEEE.